Mechanism and cellular function of Bud6 as an actin nucleation–promoting factor

Brian R. Graziano[a], Amy Grace DuPage[a], Alphee Michelot[b], Dennis Breitsprecher[a], James B. Moseley[a,*], Isabelle Sagot[c], Laurent Blanchoin[b], and Bruce L. Goode[a]

[a]Department of Biology and Rosenstiel Basic Medical Science Research Center, Brandeis University, Waltham, MA 02454; [b]Institut de Recherches en Technologie et Sciences pour le Vivant, Commissariat à l'Energie Atomique/Centre National de la Recherche Scientifique/Institut National de la Recherche Agronomique/Université Joseph Fourier, F-38054 Grenoble, France; [c]Institut de Biochimie et Génétique Cellulaires, Unité Mixte de Recherche 5095, Université de Bordeaux and Centre National de la Recherche Scientifique, F-33000 Bordeaux, France

ABSTRACT **Formins are a conserved family of actin assembly–promoting factors with diverse biological roles, but how their activities are regulated in vivo is not well understood. In *Saccharomyces cerevisiae*, the formins Bni1 and Bnr1 are required for the assembly of actin cables and polarized cell growth. Proper cable assembly further requires Bud6. Previously it was shown that Bud6 enhances Bni1-mediated actin assembly in vitro, but the biochemical mechanism and in vivo role of this activity were left unclear. Here we demonstrate that Bud6 specifically stimulates the nucleation rather than the elongation phase of Bni1-mediated actin assembly, defining Bud6 as a nucleation-promoting factor (NPF) and distinguishing its effects from those of profilin. We generated alleles of Bud6 that uncouple its interactions with Bni1 and G-actin and found that both interactions are critical for NPF activity. Our data indicate that Bud6 promotes filament nucleation by recruiting actin monomers to Bni1. Genetic analysis of the same alleles showed that Bud6 regulation of formin activity is critical for normal levels of actin cable assembly in vivo. Our results raise important mechanistic parallels between Bud6 and WASP, as well as between Bud6 and other NPFs that interact with formins such as Spire.**

Monitoring Editor
Fred Chang
Columbia University

Received: May 9, 2011
Revised: Jul 15, 2011
Accepted: Aug 23, 2011

INTRODUCTION

A wide variety of processes in eukaryotic cells are driven by the dynamic assembly and remodeling of filamentous actin networks. One of the critical control points in regulating actin cytoskeleton dynamics in vivo is the nucleation of new filaments. To block spurious actin assembly, cells express a battery of actin monomer–binding proteins (e.g., profilin) and capping proteins, which collectively suppress spontaneous growth of filaments. These physiological barriers to actin assembly are overcome by localized activation of nucleation and elongation factors (Chesarone and Goode, 2009; Dominguez, 2009). Nucleators, such as the Wiskott–Aldrich syndrome protein (WASp)–Arp2/3 complex, formins, Spire, Cobl, Lmod, JMY, and adenomatous polyposis coli (APC), catalyze the initial formation of filament "seeds" (stable nuclei consisting of multiple actin subunits), whereas elongation factors, such as formins and Ena/VASP, increase the rate of monomer addition at the growing ends of filaments. Some nucleators also depend on cofactors, or nucleation-promoting factors (NPFs), for their activities (e.g., WASp for the Arp2/3 complex). In addition, there is mounting evidence for the direct interactions and synergy between pairs of actin nucleators, including Spire–Cappuccino, Spire–Fmn2, and APC–mDia1 (Quinlan *et al.*, 2007; Okada *et al.*, 2010; Pfender *et al.*, 2011; Vizcarra *et al.*, 2011; Zeth *et al.*, 2011).

Formins are among the most widely expressed actin assembly–promoting factors and play essential roles in diverse cellular processes (Goode and Eck, 2007). The C-terminal half of formins contains two conserved domains, formin homology 1 (FH1) and FH2, which directly facilitate actin nucleation and/or elongation. The dimeric FH2 domain is critical for nucleation and remains processively

This article was published online ahead of print in MBoC in Press (http://www.molbiolcell.org/cgi/doi/10.1091/mbc.E11-05-0404) on August 31, 2011.

*Present address: Department of Biochemistry, Dartmouth Medical School, Hanover, NH 03755.

Address correspondence to: Bruce L. Goode (goode@brandeis.edu).

Abbreviations used: APC, adenomatous polyposis coli; DAD, diaphanous autoregulatory domain; FH, formin homology; NPF, nucleation-promoting factor; WASp, Wiskott–Aldrich syndrome protein; WH, WASp homology.

attached to the barbed end of the filament as it elongates, protecting it from capping proteins (Pruyne *et al.*, 2002; Sagot *et al.*, 2002; Zigmond *et al.*, 2003; Kovar and Pollard, 2004; Moseley *et al.*, 2004; Xu *et al.*, 2004). The FH1 domain recruits profilin–actin complexes and increases the efficiency of actin subunit insertion at the FH2-capped end to accelerate elongation (Romero *et al.*, 2004; Kovar *et al.*, 2006). Despite these advances, it is still not clear how formins catalyze the nucleation of an actin filament "seed." One earlier study hypothesized that the FH2 stabilizes spontaneously formed actin dimers or trimers (Pring *et al.*, 2003). However, this model does not explain how formins efficiently nucleate actin assembly in vivo, where most actin monomers are bound to other proteins such as profilin, which suppress spontaneous dimer and trimer formation. A more recent study revealed that the formin diaphanous autoregulatory domain (DAD), located C-terminal to the FH2 domain, binds to actin monomers to enhance nucleation activity (Gould *et al.*, 2011). Furthermore, this and other studies suggest that the FH1 domain may contribute to actin nucleation through its interactions with profilin–actin (Li and Higgs, 2003; Paul and Pollard, 2008). Although these mechanisms offer one explanation for how formins may overcome barriers to nucleation in vivo, they leave open the possibility of additional factors that interact with formins being involved in nucleation.

In the budding yeast *Saccharomyces cerevisiae*, the formin proteins Bni1 and Bnr1 share an overlapping, essential role in assembling actin cables, which serve as polarized tracks for myosin-dependent transport of secretory vesicles and other cargo delivered to the bud tip (Moseley and Goode, 2006). Bud6, an in vivo binding partner of Bni1, localizes to the bud tip and bud neck, and deletion of *BUD6* results in a severe loss of actin cable staining (Amberg *et al.*, 1997). Similarly, deletion of *BUD6* in *Schizosaccharomyces pombe* results in diminished staining of actin cables assembled by the formin for3p (Feierbach *et al.*, 2004). Bud6 also plays important roles in microtubule end capture to orient the mitotic spindle (Segal *et al.*, 2002) and in maintaining endoplasmic reticulum and nuclear membrane diffusion barriers between mother and daughter cells (Luedeke *et al.*, 2005; Shcheprova *et al.*, 2008). Whereas the N-terminal half of Bud6 directs its localization in vivo (Jin and Amberg, 2000) and mediates microtubule capture (Delgehyr *et al.*, 2008), the C-terminal half of Bud6 (C-Bud6; residues 489–788) binds to both the DAD region of Bni1 and G-actin (Evangelista *et al.*, 1997; Moseley *et al.*, 2004). Furthermore, C-Bud6 stimulates Bni1-mediated actin assembly in a concentration-dependent manner (Moseley *et al.*, 2004; Moseley and Goode, 2005). However, these studies left open two critical questions about Bud6. First, they did not distinguish between effects of Bud6 on the nucleation versus elongation phases of actin filament assembly, which is an important mechanistic distinction. By 2006, it was discovered that formins catalyze not only the nucleation phase of actin filament assembly, but also elongation (Kovar *et al.*, 2006), making it critical to determine which phase of actin assembly is affected by each formin regulator. Profilin promotes the elongation of formin-capped filaments (Kovar *et al.*, 2006), but the effects of Bud6 on nucleation versus elongation are unclear. Second, the importance of Bud6 effects on formin activity was not tested in vivo. Bud6 is multifunctional (see earlier discussion), and due to the unavailability of separation-of-function *bud6* alleles, it has been unclear whether the reduced levels of actin cable staining in *bud6*Δ cells stems from a loss of Bud6 effects on formins or the loss of another function of Bud6. To address these questions, we dissected the Bud6 mechanism in vitro, using bulk fluorescence and total internal reflection fluorescence (TIRF) analysis, generated separation-of-function *bud6* alleles, and analyzed their effects in vivo.

RESULTS

Bud6 strongly enhances actin nucleation by Bni1 without affecting elongation

We first purified and compared C-Bud6 (489–788) effects on C-Bni1 (FH1-FH2-C)–induced actin assembly in the presence and absence of 5 µM profilin (Figure 1, A and B). In an earlier study, we showed that C-Bud6 and low concentrations (0.2 µM) of profilin have additive effects in stimulating C-Bni1 (Moseley *et al.*, 2004). However, profilin is highly abundant in cells, present at concentrations well above monomeric actin, and inhibits nucleation. Thus the conditions used here, in which profilin suppresses spontaneous self-association of actin subunits, provide a more physiologically relevant test of the ability of Bud6 to stimulate Bni1-induced actin assembly. In these assays, we observed that C-Bud6 dramatically increased the rate of actin assembly by C-Bni1 both in the presence and absence of 5 µM profilin (Figure 1, A and B). Furthermore, these stimulatory effects were observed at different concentrations of actin (Figure 1C). As expected, C-Bud6 had no stimulatory effects on actin assembly in the absence of C-Bni1. These results suggest that Bud6 is capable of assisting Bni1 in stimulating actin filament assembly when challenged with a cellular inhibitor of nucleation, profilin.

Because bulk pyrene–actin assembly assays do not distinguish between nucleation and elongation effects on actin assembly, we next used TIRF microscopy to directly compare rates of barbed-end growth of individual actin filaments in the presence of C-Bni1 alone and C-Bni1 plus C-Bud6 or profilin (Figure 2A and Supplemental Movies S2–S4). Note that in these experiments, in which elongation rates were being measured, for the reactions containing C-Bud6 we used a lower concentration of C-Bni1 (1 instead of 2.5 nM) to control against filament crowding, which interferes with measurement of elongation. On the other hand, for the reactions containing profilin we used a higher concentration of C-Bni1 (5 nM) to counteract profilin's suppressive effects on nucleation. Consistent with previously reported effects (Kovar *et al.*, 2006), profilin increased the rate of elongation of C-Bni1–capped filaments by ~2.5-fold compared with the actin/profilin control in the absence of C-Bni1 (Figure 2, A–C). By comparison, C-Bud6 showed no significant effect on rate of elongation of C-Bni1–capped filaments either in the presence or absence of profilin (Figure 2B). In a separate set of experiments, we used TIRF to quantify the number of filaments nucleated by C-Bni1 in the presence and absence of C-Bud6 (Figure 2D and red arrows in Figure 2E). This demonstrated that C-Bud6 increases the number of C-Bni1–nucleated filaments by approximately threefold. In these reactions, the spontaneously nucleated filaments (Figure 2E, white arrows), that is, those formed independent of C-Bni1 and C-Bud6, were identified by their slower speeds of elongation and brighter fluorescence intensities (see *Materials and Methods*).

Taken together, the TIRF data suggest that C-Bud6 stimulates the nucleation but not the elongation phase of Bni1-mediated actin assembly. This is further supported by data from seeded elongation assays (Figure 2F), in which unlabeled filamentous actin (F-actin) seeds were mixed with 0.5 µM pyrene–actin monomers, and C-Bud6 did not change the rate of barbed-end growth either in the presence or absence of C-Bni1. Furthermore, the ability of C-Bud6 to stimulate nucleation rather than elongation by Bni1 was demonstrated in two-step seeded nucleation/elongation assays (Figure 2G). This assay measures the concentration of barbed ends generated and therefore provides an index of nucleation independent of elongation. In the first step of the assay, monomeric actin (2 µM) is assembled in the presence or absence of C-Bni1 ± C-Bud6 (Figure 2G, inset). In the second step, samples of reactions from the first step are removed at 50% polymer mass assembly (dotted line, inset) and added to a second

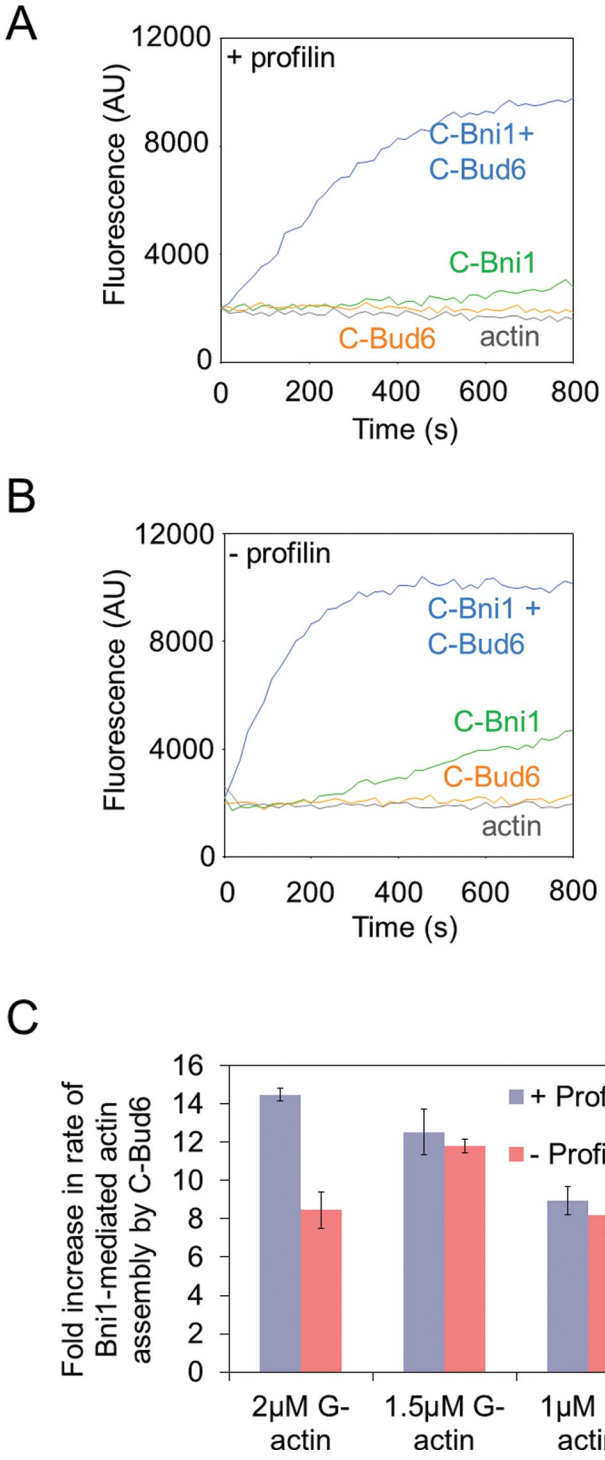

FIGURE 1: C-Bud6 strongly enhances Bni1-mediated actin assembly. (A, B) Actin monomers (2 μM, 5% pyrene labeled) were polymerized in the presence of 10 nM C-Bni1 and/or 200 nM C-Bud6, in either the presence (A) or the absence (B) of 5 μM profilin. (C) Rates of actin assembly were measured for reactions as before but in the presence of different concentrations of actin as indicated. Rates of assembly were determined from the slopes of the curves and averaged.

reaction, which contains 1 μM actin monomers. Thus filaments generated in the first reaction act as "seeds" for polymerization in the second, and the rate of assembly in the second reaction is proportional to the concentration of barbed ends produced in the first reaction. We observed minimal effects in the second reactions upon addition of seeds generated by actin alone or actin + C-Bni1 in the first reactions. However, the elongation rate increased markedly upon addition of seeds produced from first reactions containing actin + C-Bni1 + C-Bud6, suggesting that C-Bni1 + C-Bud6 had amplified barbed ends in the first reaction. These results agree with our TIRF data, and together the results indicate that Bud6 promotes Bni1-mediated actin nucleation without significantly affecting rate of elongation.

Separation of C-Bud6 interactions with Bni1 and G-actin

C-Bud6 interacts with both the DAD-containing C-terminus of Bni1 and G-actin (Amberg *et al.*, 1995; Evangelista *et al.*, 1997; Moseley *et al.*, 2004); however, the lack of *bud6* separation-of-function alleles has prevented direct tests of the relative contribution of each interaction to Bud6 activity. Using an alignment of C-Bud6 sequences from divergent fungal homologues, we identified conserved clusters of residues (Figure 3A) and generated five *bud6* alleles, mutating a total of 15 conserved residues (alanine substitutions). Two of these alleles (Bud6-3 and Bud6-5) showed partial defects individually in the same assays, so we combined them into a single hybrid allele (Bud6-35) that exhibited stronger biochemical defects. Thus, for all further biochemical analyses discussed later, we compared wild-type C-Bud6 and four mutants (Bud6-1, Bud6-35, Bud6-6, and Bud6-8), each expressed and purified from *Escherichia coli* (Figure 3B).

We first used bead pull-down assays to compare the abilities of soluble wild-type and mutant C-Bud6 to bind 6His-tagged C-Bni1 immobilized on Ni-NTA beads (Figure 3, C and D). In these assays, C-Bud6-8 displayed wild type–like binding to C-Bni1, C-Bud6-35 failed to interact with C-Bni1, and the two remaining mutants (C-Bud6-1 and C-Bud6-6) showed partial defects in binding.

Next we assessed C-Bud6 interactions with G-actin by comparing the abilities of wild-type and mutant C-Bud6 to inhibit spontaneous polymerization of actin monomers (Figure 4). As previously described (Moseley *et al.*, 2004), C-Bud6 binds specifically to G-actin (but not F-actin) and inhibits spontaneous self-association of monomers, suppressing actin polymerization in a concentration-dependent manner (Supplemental Figure S1, A and B). We tested mutant C-Bud6 polypeptides at concentrations of wild-type C-Bud6 that strongly suppress polymerization (4 μM C-Bud6 and 3 μM actin), where mutant effects would be readily apparent. This analysis revealed that Bud6-35 and Bud6-6 have wild type–like interactions with G-actin, whereas Bud6-1 and Bud6-8 show significantly weakened interactions with G-actin (Figure 4).

In summary, we obtained two Bud6 mutants with clear separation-of-function defects in vitro (summarized in Figure 5D). Whereas Bud6-35 is defective specifically in binding Bni1 but not G-actin, Bud6-8 is defective specifically in binding G-actin but not Bni1. By comparison, Bud6-1 and Bud6-6 showed partial and/or mixed defects in binding Bni1 and G-actin. Thus Bud6-35 and Bud6-8 provided ideal tools for further dissecting Bud6 mechanism and cellular function.

Interactions of C-Bud6 with both Bni1 and G-actin are required for its NPF activity

We next used the mutants identified earlier to directly test the importance of Bud6 interactions with Bni1 and G-actin for its actin nucleation activity. Rates of Bni1-induced actin assembly were measured in pyrene–actin assays over a range of C-Bud6 concentrations (0–200 nM). Higher concentrations of C-Bud6 were not tested because they sequester free actin monomers and thus nonspecifically inhibit polymerization (Moseley *et al.*, 2004). Wild-type C-Bud6 increased the rate of Bni1-mediated actin assembly in a concentration-dependent manner (Figure 5, A and C), whereas the

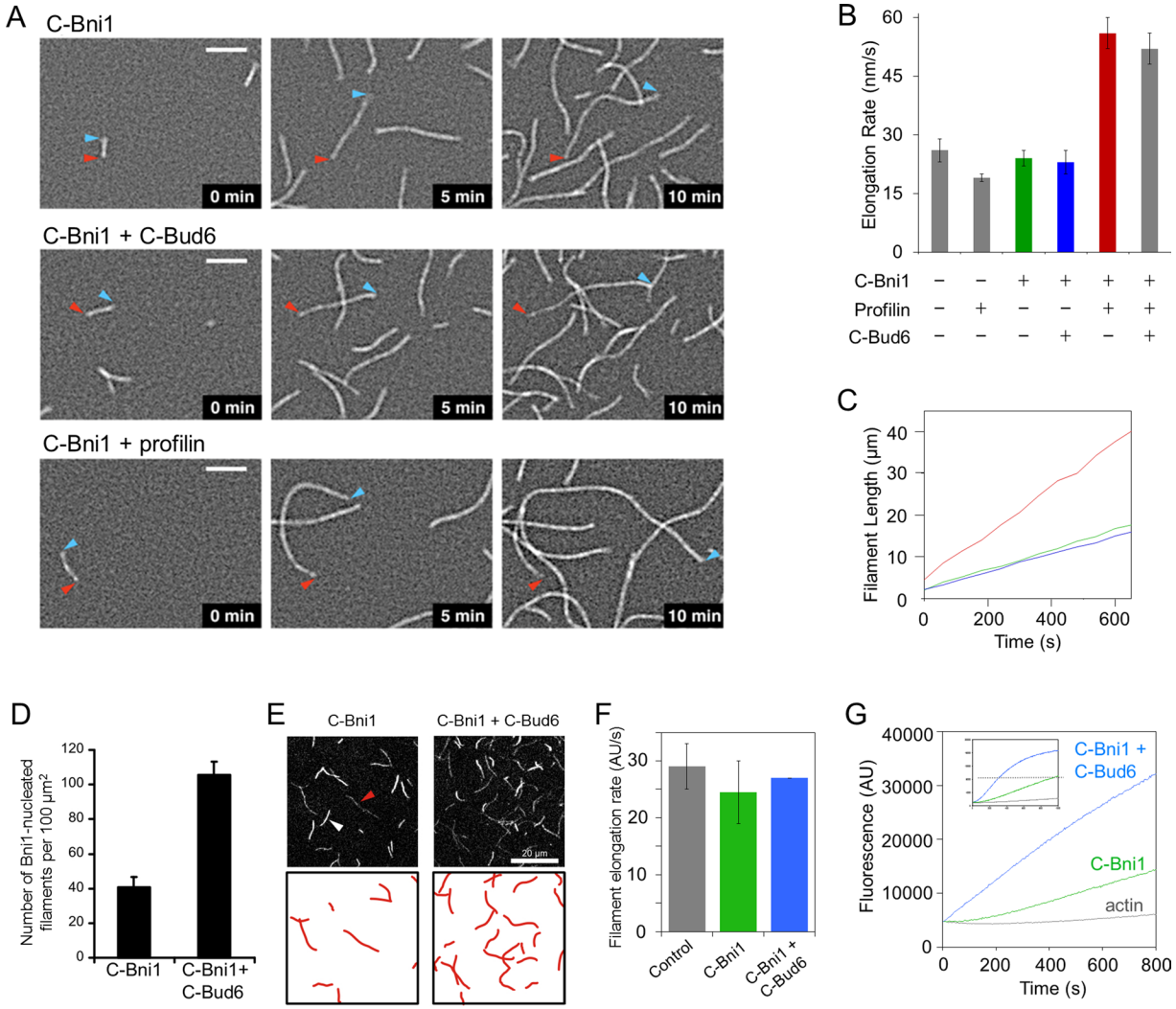

FIGURE 2: C-Bud6 stimulates actin nucleation but not elongation. (A) Time-lapse TIRF microscopy comparing barbed-end elongation rates. Reactions contained 1.2 μM monomeric actin, different concentrations of C-Bni1 (top, 2.5 nM; middle, 1 nM; bottom, 5 nM; explained in *Results*), and 200 nM C-Bud6 or 3.6 μM profilin. Time points indicated. (B) Average rates of elongation (n = 10 filaments). Colored bars correspond to reactions in A. Gray bars are controls. (C) Examples of individual filaments increasing in length over time, color coded as in B. (D) Average rates of elongation measured in seeded elongation assays (error bar for C-Bni1 + C-Bud6 is small). (E) Two-step nucleation/elongation assays. First reactions contained 2 μM actin monomers ± 20 nM C-Bni1 ± 200 nM C-Bud6. Samples were removed at 50% polymerization (dotted line, inset) and used to seed a second reaction containing 1 μM actin monomers (10% pyrene labeled). (F) Quantification of number of Bni1-generated filaments by TIRF. (G) Example images from these experiments, in which Bni1-generated filaments (red arrowhead) are distinguished from spontaneously generated filaments (white arrowhead) due their threefold-faster elongation rates and reduced fluorescent intensities (see *Materials and Methods*). Bottom, highlighted Bni1-generated filaments (red lines).

four mutants of C-Bud6 each showed severely impaired effects (Figure 5, B and C, and Supplemental Figure S2, A and B). The observation that Bud6-35 and Bud6-8 mutants failed to stimulate actin nucleation demonstrates that Bud6 NPF activity depends critically on its interactions with both Bni1 and G-actin. These findings suggest that Bud6 stimulates nucleation by recruiting actin monomers to Bni1.

In vivo mechanism of Bud6 in promoting actin cable assembly

Earlier studies showed that *bud6*Δ cells have greatly diminished levels of actin cable staining (Amberg *et al.*, 1997); however, until now it has not been possible to test whether this phenotype is due to the specific loss of Bud6 activity in stimulating formin-mediated actin assembly. Furthermore, it has not been clear whether Bud6 function in actin cable assembly requires its direct interactions with Bni1 and/or G-actin. To address these issues, we integrated our two separation-of-function alleles, *bud6-35* (formin-binding defective) and *bud6-8* (actin-binding defective) in haploid strains. Each construct included a 3xHA tag at the C-terminus, allowing verification of expression on immunoblots of whole-cell extracts (Figure 6A). A wild-type *BUD6-HA* allele was integrated in parallel and used as the control strain in all of the analyses that follow.

We first compared wild-type and mutant haploid strains, alongside an isogenic *bud6*Δ strain, for defects in cell growth at different temperatures after serial dilution and plating (Figure 6B). As previously reported, *bud6*Δ cells grew normally at these temperatures (Jaquenoud and Peter, 2000). Surprisingly, however, growth defects

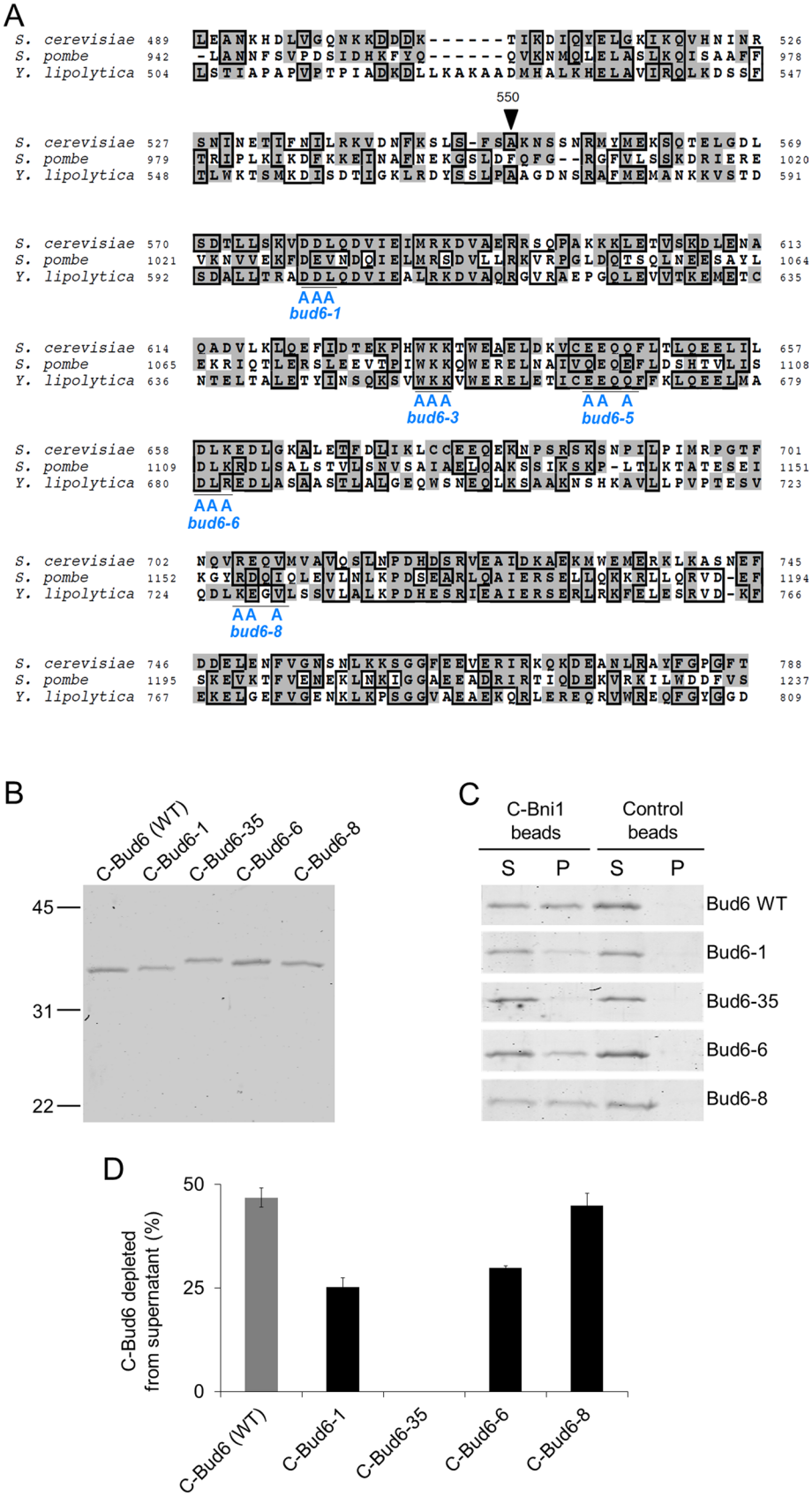

FIGURE 3: Wild-type and mutant C-Bud6 interactions with Bni1. (A) Alignment of amino acid sequences in the C-terminal halves of fungal homologues of Bud6. Residues shaded in gray are conserved; those that were mutated to create the *bud6* alleles are designated with a blue A. *bud6-3* and *bud6-5* were combined to produce *bud6-35*. (B) Coomassie-stained gel of purified wild-type and mutant C-Bud6 (489–788) polypeptides. Each lane contains ~100 ng of protein. (C) Bead pull-down assays. Beads coated with 6His-C-Bni1 (1 μM final) or empty control beads were incubated for 10 min with soluble C-Bud6 polypeptides (1 μM final) and then centrifuged. Samples of supernatants (S) and pellets (P) were analyzed on gels by Coomassie staining. (D) Percentage of C-Bud6 depleted from the supernatants by Bni1-coated beads. Each bar represents an average of two independent trials. Error bars, SD.

were observed at 34 and 37°C for both the *bud6-35* and *bud6-8* strains, with *bud6-35* showing a slightly stronger growth phenotype. We also compared F-actin organization in fixed wild-type and mutant cells by Alexa 488–phalloidin staining (Figure 6C). In wild-type cells, thicker actin cables filled the mother, and smaller cables were present in the bud but more difficult to detect due to the intense actin patch staining. In contrast, *bud6*Δ cells displayed a substantial loss of cable staining in the mother, and we rarely detected cables in the bud. These defects in F-actin organization were consistent with previous reports (Amberg *et al.*, 1997; Delgehyr *et al.*, 2008). By comparison, *bud6-35* and *bud6-8* cells showed a stronger loss of actin cable staining and more depolarized actin patches than *bud6*Δ cells, in agreement with their more severe growth defects. These actin phenotypes were quantified by scoring populations of cells from each strain (Figure 6D), using similar criteria as described previously (Delgehyr *et al.*, 2008).

Because of the unexpected nature of this observation—that the point mutations in *bud6* cause stronger phenotypes than the gene deletion—we further tested whether *bud6-35* and *bud6-8* alleles are dominant or recessive in diploids. We generated heterozygous and homozygous diploid strains (*BUD6/BUD6*, *BUD6/bud6*Δ, *BUD6/bud6-35*, *BUD6/bud6-8*, *bud6*Δ*/bud6*Δ, *bud6*Δ*/bud6-35*, *bud6*Δ*/bud6-8*, *bud6-35/bud6-35*, and *bud6-8/bud6-8*) and compared their cell growth (Figure 7A) and actin organization (Figure 7, B and C), scoring the actin phenotypes as before (Figure 7D). This analysis indicated that the *bud6-35* and *bud6-8* alleles are recessive, as demonstrated by the heterozygotes (*BUD6/bud6-35* and *BUD6/bud6-8*) growing as well as wild-type cells and having actin organization equivalent to *BUD6/bud6*Δ. On the other hand, the alleles showed some characteristics of dose-responsive toxicity. Specifically, homozygous *bud6-35/bud6-35* and *bud6-8/bud6-8* strains showed stronger defects in cell growth and actin

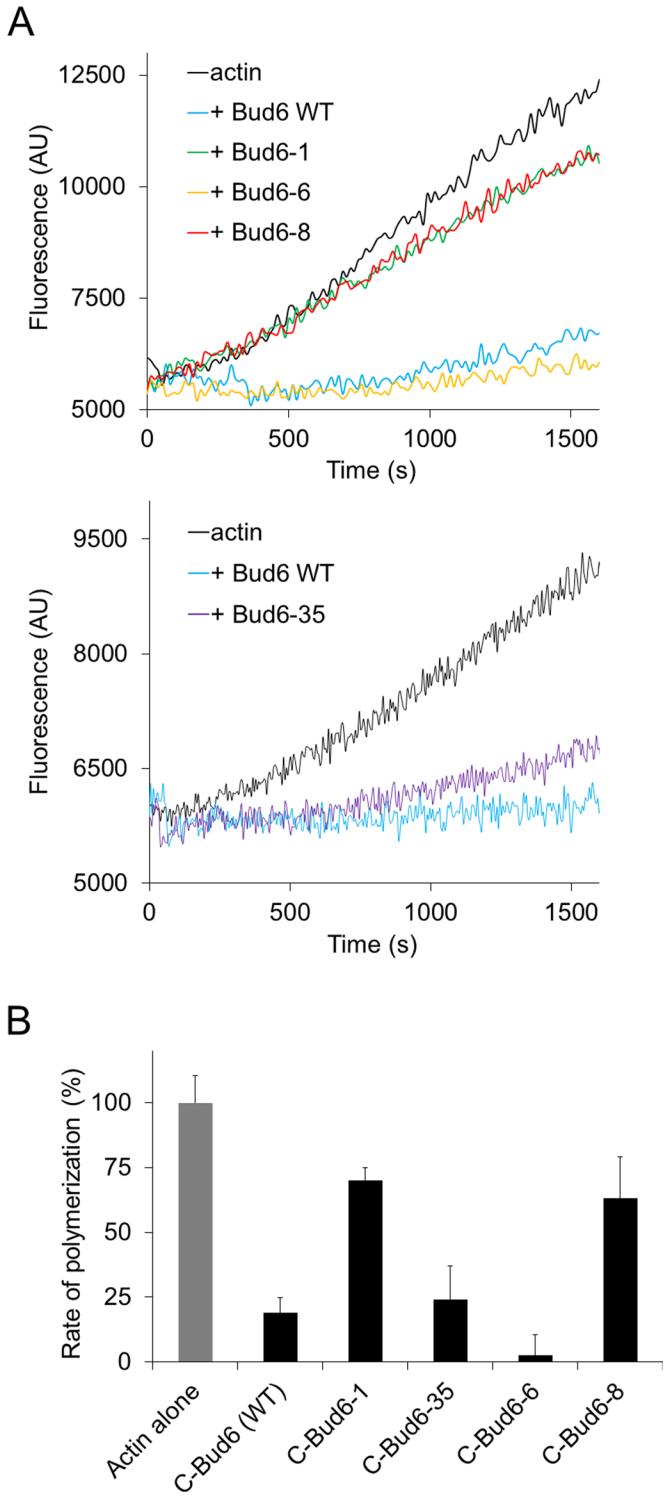

FIGURE 4: Wild-type and mutant C-Bud6 interactions with G-actin. (A) Polymerization of 3 µM monomeric actin (5% pyrene labeled) in the presence of 4 µM wild-type or mutant C-Bud6 polypeptide. (B) Quantification of data as in A. Assembly rates for reactions containing actin + C-Bud6 were normalized to rates for reactions containing actin alone. Rates were determined from the slopes of the curves and averaged from three independent trials. Error bars, SD.

organization than *bud6Δ/bud6Δ*, *bud6Δ/bud6-35*, or *bud6Δ/bud6-8* strains. The differences in actin organization of *bud6-35/bud6-35* and *bud6-8/bud6-8* compared with *bud6Δ/bud6Δ* were even more pronounced at 37°C (Figure 7D) and revealed a correlation between loss of cable staining and defective cell growth.

DISCUSSION

Bud6 and profilin have distinct functions in formin-mediated actin assembly

Until now, the molecular mechanism and cellular function of Bud6 as an actin assembly-promoting factor were unclear. Our findings provide important new insights. Biochemically, we showed that Bud6 stimulates the nucleation rather than the elongation phase of Bni1-mediated actin assembly, defining it as an NPF. In addition, we demonstrated that the NPF activity of Bud6 requires distinct physical interactions with both G-actin and the DAD-containing C-terminus of Bni1. Together, these biochemical observations indicate that Bud6 stimulates filament nucleation by recruiting actin monomers to the DAD region of the formin. In contrast, profilin promotes filament elongation (Romero *et al.*, 2004; Kovar *et al.*, 2006). Therefore Bud6 and profilin have distinct, complementary mechanistic roles in promoting actin assembly, explaining the mechanistic basis for their previously reported synthetic lethal interaction (Moseley *et al.*, 2004). This view of Bud6 and profilin making distinct contributions to actin assembly is also consistent with structural data. In the profilin–actin cocrystal structure, profilin associates with the "barbed end" of the actin monomer, leaving the pointed end free to associate with the barbed end of an actin filament (Figure 8A). As such, profilin–actin interactions are predicted to sterically interfere with the FH2 domain's ability to engage the barbed ends of actin subunits during nucleation. On the other hand, profilin is not predicted to interfere with elongation, because in the FH2 domain "open" state (when only half of the FH2 dimer is bound to actin subunits at the barbed end), profilin–actin can be readily added to the filament end (Figure 8C). In contrast to profilin, the Bud6-binding footprint on actin (Figure 8A) (Amberg *et al.*, 1995) predicts that Bud6 binds to the side and/or pointed end of the actin monomer, making it less likely to sterically interfere with the FH2 during nucleation. This agrees with our observation that Bud6 enhances Bni1-dependent nucleation even in the presence of high levels of profilin (Figure 1).

What is the mechanism underlying Bud6 NPF activity? Because each FH2 dimer has two C-terminal extensions with DAD domains (Nezami *et al.*, 2010; Otomo *et al.*, 2010), we postulate that at least two Bud6 molecules bind to each formin (Figure 8C). As such, Bud6 would recruit and position multiple actin monomers in close proximity to each other to facilitate actin self-association. This would occur near the FH2 domain to increase the efficiency of barbed-end capture (Otomo *et al.*, 2005). After nucleation, the recruitment of profilin–actin subunits to the FH1 domain would accelerate elongation at the FH2-capped barbed end. It is interesting that Bud6 binds to Bni1 at a site very near or overlapping with the DAD domain, since we have recently shown that the DAD domain of mDia1 binds to G-actin and enhances nucleation (Gould *et al.*, 2011) and that the DAD-containing C-terminus of Bni1 binds G-actin and may contribute similarly to actin assembly. Future work will be required to determine whether Bud6 and Bni1 DAD can bind simultaneously to G-actin or instead Bud6 "replaces" the DAD, providing a higher-affinity G-actin recruitment site. Regardless of which is the case, our data show that Bud6 strongly stimulates nucleation of actin assembly by C-Bni1 (FH1-FH2-DAD), an effect that requires Bud6 interactions with DAD.

Unifying properties of nucleation-promoting factors

Our results point to some interesting and unexpected parallels between Bud6 and WASp. Bud6 and WASp each have no effect on

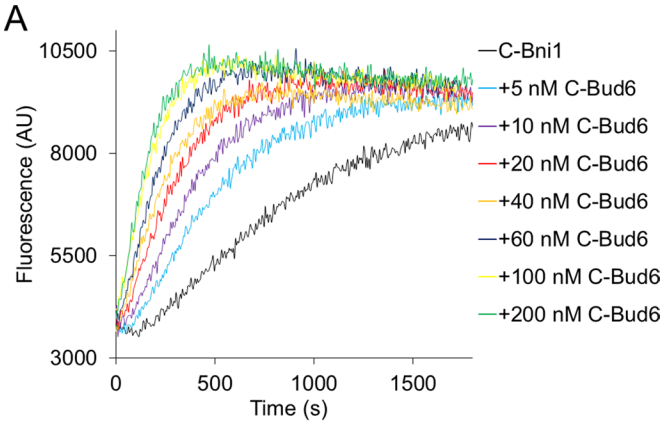

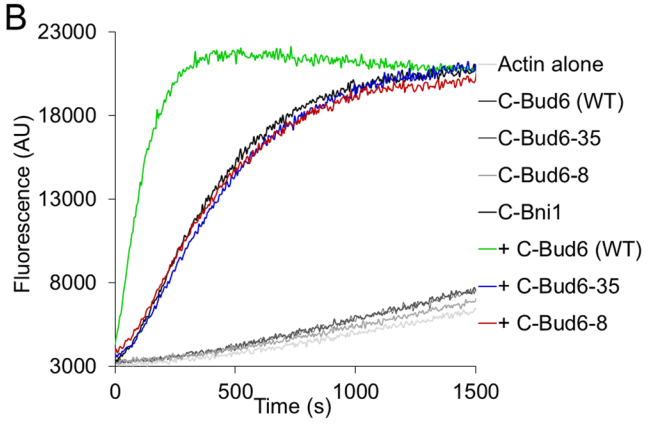

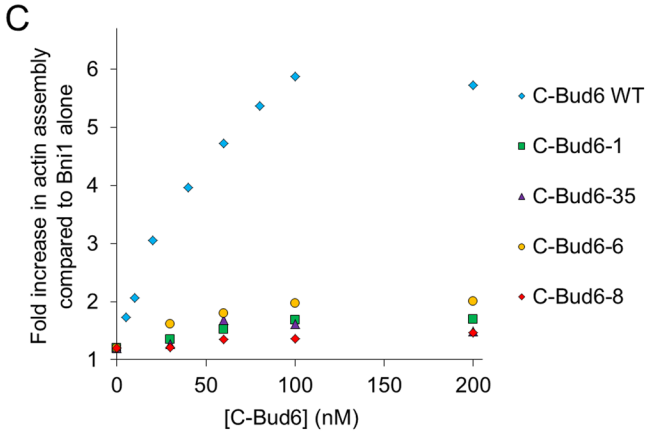

D

	G-actin binding	C-Bni1 binding	Nucleation activity
C-Bud6 WT	+	+	+
C-Bud6-1	-	+/-	-
C-Bud6-35	+	-	-
C-Bud6-6	+	+/-	-
C-Bud6-8	-	+	-

FIGURE 5: Wild-type and mutant C-Bud6 effects on Bni1-mediated actin assembly. (A) Concentration-dependent effects of wild-type C-Bud6 on the assembly of 2 µM monomeric actin (5% pyrene labeled) by 10 nM C-Bni1. (B) Comparison of the effects of 200 nM wild-type or mutant C-Bud6 on actin assembly by 10 nM C-Bni1 as in A. (C) Concentration-dependent effects of wild-type and mutant C-Bud6 on rate of actin assembly by 10 nM C-Bni1 as in A. Rates determined from slopes of raw curves in A and in Supplemental Figure S2, A and B, and similar data sets for C-Bud6-1 and C-Bud6-6. Each data point on the graphs is an average of at least two independent trials. To calculate fold increase (*y*-axis), rate of actin assembly for C-Bud6 + C-Bni1 was divided by rate of actin assembly for C-Bni1 alone. (D) Summary table of data from Figures 3–5.

nucleation in the absence of other factors but have strong NPF activity when bound to their ligands—formins and Arp2/3 complex, respectively. Thus, for each nucleation system (Bud6–Bni1 and WASp–Arp2/3), robust activity requires both an actin monomer–binding protein and a high-affinity filament end-capturing protein. A second similarity between Bud6 and WASp is that they each use WASp homology 2 (WH2) domains to bind G-actin. Our *bud6-8* allele, which abolishes G-actin binding, falls within a WH2-like sequence in Bud6 (residues 704–725) (Figure 8B). Similarly, it has been shown that WASp NPF activity depends on its WH2 domain–binding actin (Higgs *et al.*, 1999). WH2 domains are found in a variety of actin regulators (Qualmann and Kessels, 2009) and consist of a short α-helix followed by a cluster of basic residues, with both elements contributing to G-actin binding (Dominguez, 2009). *bud6-8* contains mutations of several conserved residues within the predicted α-helix (Figure 8C). The utilization of a WH2-like domain by Bud6 may also explain why Bud6 NPF activity is robust in the presence of profilin (Figure 1), since some WH2 domains and profilin can bind simultaneously to G-actin (Ferron *et al.*, 2007). Taken together, our findings draw intriguing links between these two nucleation systems (Arp2/3 and formins), which until now had been viewed as having unrelated mechanisms. Moreover, the observation that Bud6 uses a WH2-like domain to bind G-actin and stimulate nucleation reveals that it has common properties shared by a wide variety of nucleators. WH2-related domains have been shown to play a critical role in six of seven eukaryotic actin nucleators (WASp-Arp2/3, Spire, Lmod, Cobl, JMY, and formin-Bud6) and many of their bacterial counterparts (VopF, VopL, and TARP) (Dominguez, 2007; Qualmann and Kessels, 2009). Thus the presence of WH2-like actin monomer–binding domains may be the most conserved feature among actin nucleators.

One important question raised by our observations is, how conserved is the nucleation cofactor strategy illustrated by Bud6-Bni1 in other formins? Recent genetic and/or biochemical studies point to a growing number of formins that directly collaborate with other nucleators or NPFs to promote actin assembly. These include Capu/Fmn2–Spire (Quinlan *et al.*, 2007), mDia1–APC (Wen *et al.*, 2004; Okada *et al.*, 2010), Daam1–flightless (Higashi *et al.*, 2010), and now Bni1–Bud6. In addition, there is evidence indicating that Arp2/3 complex and formins collaborate to promote filopodia formation (Yang *et al.*, 2007; Lee *et al.*, 2010). In each of these examples, the formin's processive capping and barbed-end protection activity is paired with an actin monomer–binding nucleator or NPF. This strategy of combining two factors with complementary activities may be highly beneficial in a cellular environment in which there are abundant suppressors of actin nucleation (Chesarone and Goode, 2009). In principle, this scheme also provides cells with tighter control over actin assembly, since each nucleator or NPF can be regulated independently so that a convergence of signal inputs is required for actin assembly (Prehoda *et al.*, 2000). Thus, although Bud6 shares no sequence homology with other formin NPFs outside of having a WH2-like domain, it may serve as a yeast functional counterpart. In this regard, it is interesting to note that Bud6 and Spire both interact with the C-terminal tail regions of formins (Pechlivanis *et al.*, 2009)

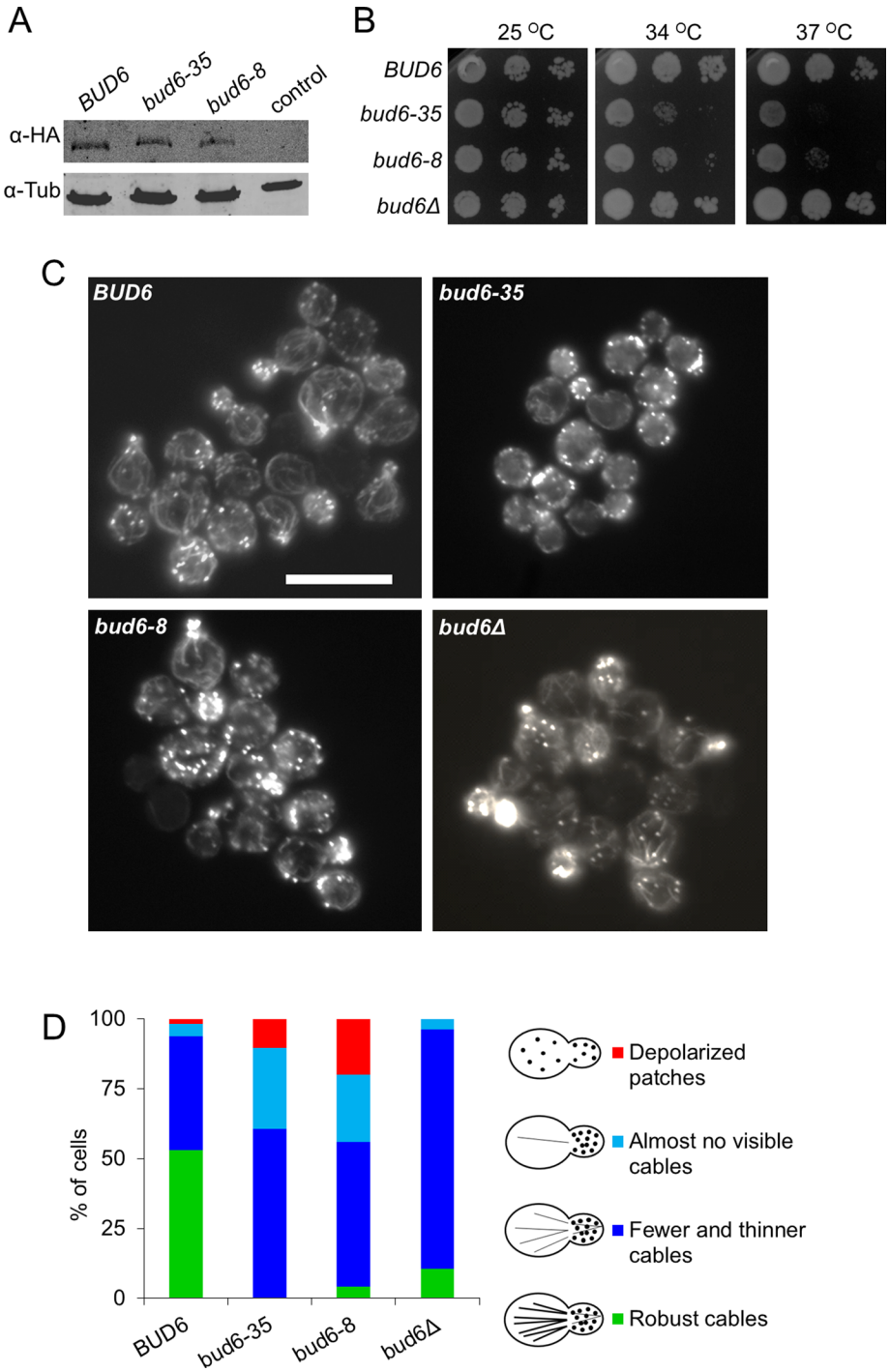

FIGURE 6: Effects of *bud6* alleles on cell growth and actin organization in haploids. (A) Immunoblot of whole-cell extracts from haploid strains, probed with anti-hemagglutinin and anti-tubulin antibodies (loading control). The control lane is from a wild-type strain expressing Bud6 with no tag. (B) Strains were serial diluted and grown at 25, 34, and 37°C on YEPD plates. (C) The strains were grown to log phase at 25°C, fixed, and stained with Alexa 488–phalloidin. Scale bar, 10 μm. (D) Quantification of F-actin phenotypes after fixation and actin staining as in C. For each strain, >200 budded cells were scored and categorized as follows: 1) Robust cables in mother; cables sometimes visible in bud; polarized patches. 2) Fewer and thinner cables in the mother, sometimes with a disorganized appearance; cables occasionally visible in bud; polarized patches. 3) Very few visible cables in the mother; no cables in bud; polarized patches. 4) No visible cables in the mother or bud; depolarized patches.

and both regulate not only formin-mediated actin assembly, but also microtubule dynamics (Theurkauf, 1994; Rosales-Nieves *et al.*, 2006; Dahlgaard *et al.*, 2007).

In vivo function of Bud6 as an NPF

Until now it has not been possible to attribute specific phenotypes of *bud6Δ* cells (e.g., loss of actin cables and polarity) with the loss of individual activities of Bud6, since Bud6 is a multifunctional protein with roles in actin cable formation, polarized cell growth, capture of astral microtubule plus ends, and maintenance of endoplasmic reticulum and nuclear membrane diffusion barriers. We have overcome this barrier by introducing point mutations into the C-terminal half of Bud6 to produce separation-of-function alleles. These tools allowed us to directly test the in vivo importance of Bud6 interactions with G-actin and formins (and its NPF activity) for actin cable formation and polarized cell growth. Our data show that both of the interactions are critical for Bud6 function in actin cable assembly, strongly supporting the role of Bud6 as an NPF in vivo. These tools may also prove useful in future studies for testing the importance of Bud6 NPF activity in its other cellular functions.

Of interest, *bud6-35* and *bud6-8* alleles led to more severe defects in actin cable assembly and cell growth than a complete deletion of the *BUD6* gene in haploids. These observations suggested that the alleles were dominant or recessive gain-of-function alleles. To distinguish between these two possibilities, we further generated mutant homozygous and heterozygous diploid strains and compared their cell growth and actin organization. This analysis revealed that *bud6-35* and *bud6-8* are recessive gain-of-function alleles. The alleles were never dominant over a wild-type copy of *BUD6*, and their toxicity in diploids was only observed when there were two copies of the mutant allele. At this point, it is not clear why the allele toxicity is dose dependent or why the alleles result in a gain of function, that is, they are more harmful to cell growth and actin organization than *bud6Δ*. One possibility for the latter is that a full deletion of *BUD6* leads to changes in the expression levels of other proteins that partially compensate for the loss of Bud6 function. Future work is needed to address this and other possibilities.

Finally, although our data provide new clarity concerning the role of Bud6 in regulating Bni1 activity, they leave the function and mechanism of Bud6 in regulating Bnr1 to be determined. Previous studies showed that purified Bud6 (residues 447–788) binds directly to Bnr1 (residues 757–1374; Kikyo *et al.*, 1999), and in vivo the deletion of *BUD6* in *bni1Δ* cells leads to further loss of actin cables and synthetic growth defects (Tong *et al.*, 2001; Delgehyr *et al.*, 2008). Together, these observations strongly

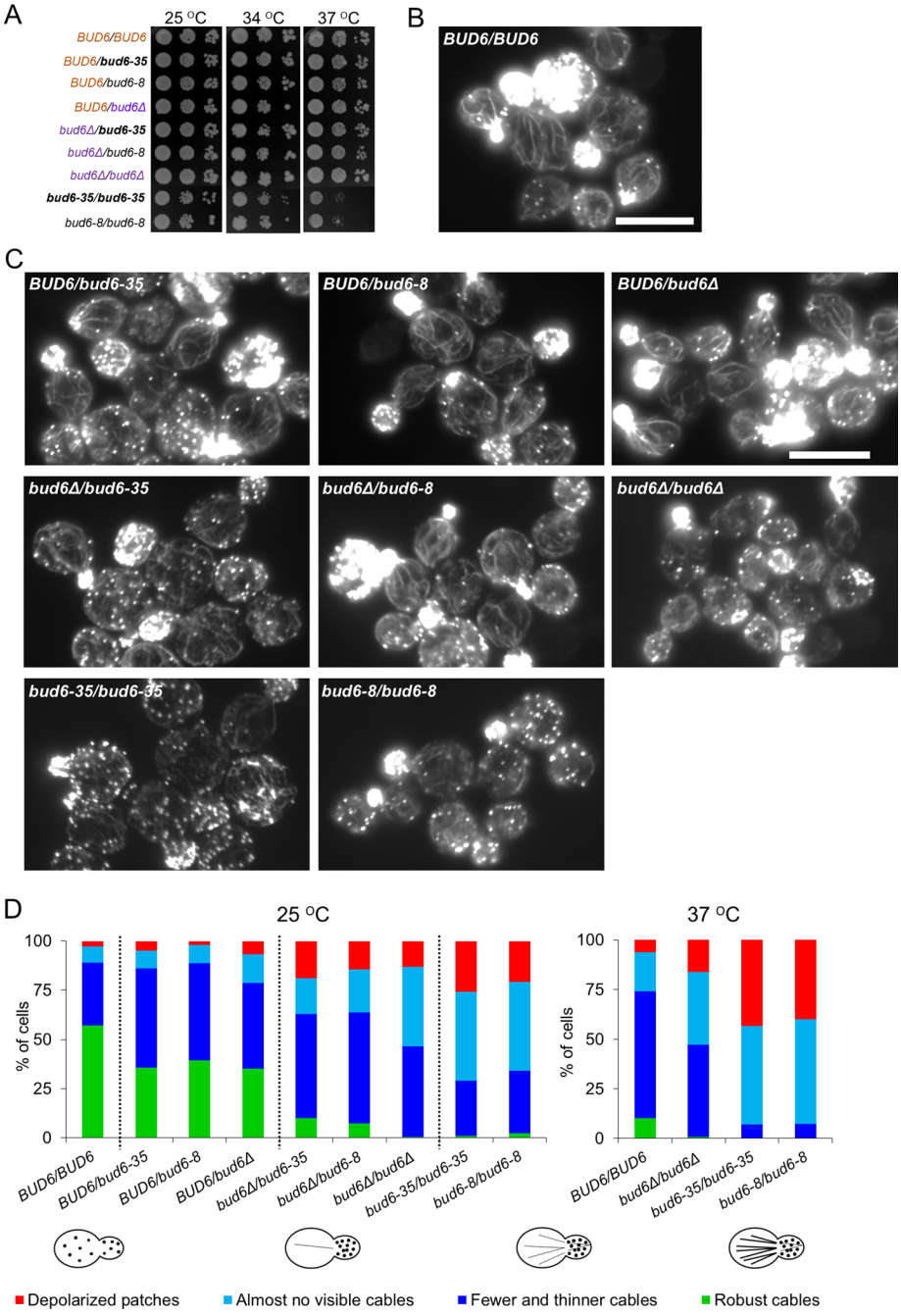

FIGURE 7: Effects of *bud6* alleles on cell growth and actin organization in diploids. (A) Diploid strains were serial diluted and grown at 25, 34, and 37°C on YEPD plates. (B, C) The strains were grown to log phase at 25°C, fixed, and stained with Alexa 488–phalloidin. Scale bars, 10 μm. (D) Quantification of F-actin phenotypes. Cells were grown to log phase at 25°C, then fixed and stained with Alexa 488–phalloidin as in B and C, or shifted to 37°C for an additional 2 h before fixation. For each strain, >200 budded cells were scored and categorized as in Figure 6D.

suggest that Bud6 has some role in promoting Bnr1-dependent actin cable formation. However, our previous biochemical analysis of Bud6 (489–788) showed that it had no effect on C-Bnr1 actin assembly activity (Moseley and Goode, 2005). Thus it waits to be seen whether and how Bud6 directly stimulates Bnr1 activity to promote cable formation. One clue from our data is that the *bud6-35* and *bud6-8* alleles, which disrupt DAD and G-actin binding, respectively, exhibit far stronger loss-of–actin cable phenotypes than *bni1Δ*. The specific nature of these alleles suggests that Bud6 promotes Bnr1-dependent actin cable assembly in vivo by a mechanism related to that shown here for Bni1. However, functional effects of Bud6 on Bnr1 may require additional factors and/or posttranslational modifications that are lacking in our purified system. Resolving this mechanism is an important future goal.

MATERIALS AND METHODS

Plasmids and strains

The vectors used in this study for expressing 6His-C-Bni1 (1227–1953) and GST-C-Bud6 (489–788) have been described (Moseley *et al.*, 2004; Moseley and Goode, 2005). The C-Bud6 vector was modified further by site-directed mutagenesis to generate plasmids used to express and purify Bud6-1, Bud6-3, Bud6-5, Bud6-35, Bud6-6, and Bud6-8 from *E. coli*. For in vivo mutant analyses, we first integrated an in-frame 3xHA tag (marked with *HIS3*) at the 3′ end of the *BUD6* open reading frame (ORF; Longtine *et al.*, 1998) in a wild-type strain of w303 background (BGY12: *MATα; his3-11,15; ura3-53; leu2-3,112; ade2-1; trp1-1; psi+; ssd-; GAL+*), producing a new strain, BGY1410. Bud6-3xHA was previously shown to complement Bud6 function in vivo (Moseley and Goode, 2005). Next the wild-type *BUD6-3xHA* ORF plus 300 base pairs 5′ UTR and 200 base pairs 3′ UTR (including the *HIS3* marker) was PCR amplified from genomic DNA and cloned into the pRS315 vector (Sikorski and Hieter, 1989) using *Xho*I and *Not*I sites. This plasmid was used as a template for site-directed mutagenesis to generate integration vectors for *bud6-35* and *bud6-8*. For integrations, DNA fragments encoding for amino acids 550–788 and the 3xHA tag, along with 200 base pairs 3′ UTR and the marker were amplified from the plasmids and transformed into BGY12, producing BGY1411 (*bud6-35-3xHA::HIS3*) and BGY1412 (*bud6-8-3xHA::HIS3*). All plasmids were verified by DNA sequencing, and all integrations were verified by sequencing the PCR-amplified ORFs. The haploid strains generated (BGY1411, BGY1412, and BGY1410) and BGY1413 (*bud6Δ::TRP1*, isogenic to BGY12) were each genetically crossed to BGY10 (*MATa*, isogenic to BGY12) to produce these heterozygous diploid strains: BGY1414 (*BUD6/BUD6-3xHA::HIS3*), BGY1415 (*BUD6/bud6Δ::TRP1*), BGY1416 (*BUD6/bud6-35-3xHA::HIS3*), and BGY1417 (*BUD6/bud6-8-3xHA::HIS3*). These strains were sporulated to produce the following haploid strains: BGY1418 (*MATa, bud6Δ::TRP1*), BGY1419 (*MATa, bud6-35-3xHA::HIS3*), and BGY1420 (*MATa, bud6-8-3xHA::HIS3*). BGY1418, BGY1419, and BGY1420 were crossed to BGY1413, BGY1411, and BGY1412, respectively, to generate the following homozygous diploid strains: BGY1421 (*bud6Δ::TRP1/bud6Δ::TRP1*), BGY1422 (*bud6-35-3xHA::HIS3/bud6-35-3xHA::HIS3*), and BGY1423 (*bud6-8-3xHA::HIS3/bud6-8-3xHA::HIS3*). The

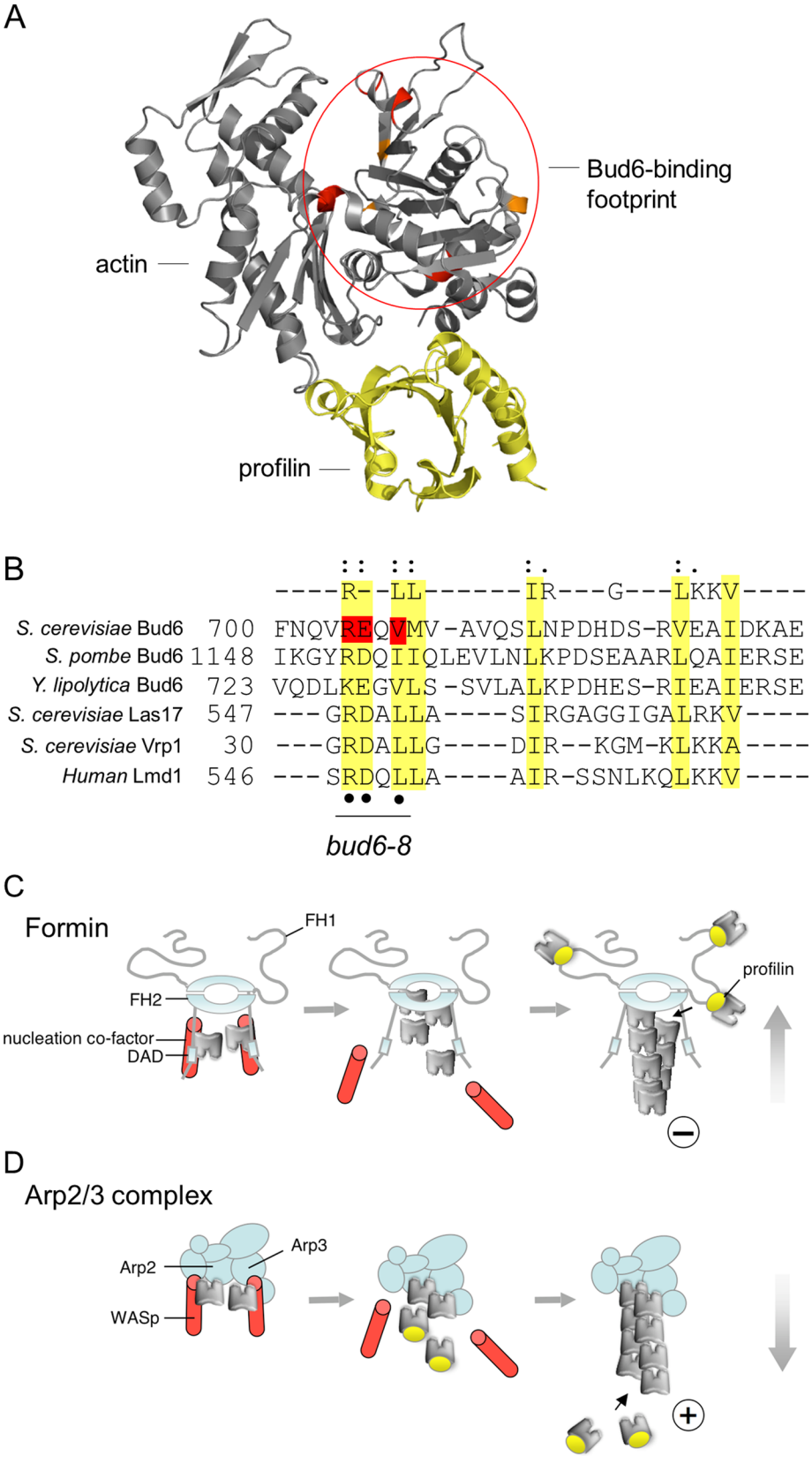

FIGURE 8: Model for Bud6 function as an NPF. (A) Cocrystal structure of profilin (yellow) bound to G-actin (gray) with the Bud6 binding footprint highlighted (red circle). Surfaces on actin essential for Bud6–actin interactions in two-hybrid assays (Amberg et al., 1997) are red; residues that make lesser contributions to the interaction are orange. (B) Alignment of WH2-like sequence in Bud6 homologues and WH2 sequences in other proteins. Yellow, conserved residues; red, residues mutated in *bud6-8*. (C) Model for Bud6 mechanism. C-Bud6 (red cylinders) uses its WH2-like domain to bind G-actin (gray) and a separate binding site to interact with the Bni1 DAD. This positions actin monomers near the FH2 (blue) to promote nucleation, catalyzing formation of actin dimers that are captured by the FH2. Bud6 dissociates, and elongation proceeds with the FH1-domain recruiting profilin (yellow)-bound actin monomers to accelerate barbed-end growth. (D) Arp2/3 complex (blue) interacts with two molecules of WH2 domain–containing WASp (red cylinders; Padrick et al., 2008), which recruit actin monomers to promote nucleation by the filament end–capturing Arp2/3 complex. Although formins and Arp2/3 complex capture opposite ends of the filament, elongation proceeds in both cases by barbed-end addition.

heterozygous diploid strains BGY1447 (*bud6Δ::TRP1/bud6-35*) and BGY1448 (*bud6Δ::TRP1/bud6-8*) were created by crossing BGY1413 to BGY1419 and BGY1420, respectively.

Protein purification

Rabbit skeletal muscle actin (RMA) and *S. cerevisiae* profilin were purified as described (Spudich and Watt, 1971; Moseley *et al.*, 2004), and RMA was labeled with pyrenyliodoacetamide (Pollard and Cooper, 1984). C-Bni1 (1227–1953) was expressed in *S. cerevisiae* strain BJ2168 as a 6His-fusion and purified as described (Moseley *et al.*, 2006) with two minor modifications: expression was induced for 6–8 h, and proteins were gel filtered into HEKG$_5$D (20 mM 4-(2-hydroxyethyl)-1-piperazineethanesulfonic acid [HEPES], pH 7.5, 1 mM EDTA, 50 mM KCl, 5% [vol/vol] glycerol, and 1 mM dithiothreitol [DTT]). C-Bud6 (489-788) was expressed in *E. coli* strain BL21 DE3, grown to mid-log phase (OD_{600} = 1.0) in 1 l of TB (12 g of tryptone, 24 g of yeast extract, 0.4% [vol/vol] glycerol, 17 mM KH_2PO_4, 72 mM K_2HPO_4) at 37°C and induced with isopropyl-β-D-thiogalactoside for 4 h. Cells were harvested and frozen at −80°C, then later thawed and resuspended in lysis buffer (50 mM Tris, pH 8.5, 150 mM NaCl, 5 mM EDTA, 1.5% sarkosyl, 5 mM DTT, standard protease inhibitors). A small amount of lysozyme was added to cell suspensions, and they were incubated on ice for 5–10 min. DNase I was added, and lysates were incubated on ice for an additional 5–10 min. Cell lysates were then sonicated and centrifuged at 15,000 × *g* for 10 min at 4°C. The supernatant was harvested and mixed with Triton X-100, final concentration 3.3% (vol/vol), and then added to 1 ml of glutathione

agarose preswollen in phosphate-buffered saline (PBS; 137 mM NaCl, 2.7 mM KCl, 4.3 mM Na_2HPO_4, 1.47 mM KH_2PO_4, pH 7.4). After 4 h of incubation at 4°C, the beads were washed four times with PBS and then twice with HEKD (20 mM HEPES, pH 7.5, 1 mM EDTA, 50 mM KCl, 1 mM DTT). Untagged C-Bud6 was released from beads by digestion with TEV protease for 2 h at room temperature and then aliquoted and snap-frozen in liquid nitrogen.

Pyrene–actin assembly assays

To prepare monomeric actin, pyrene-labeled RMA and gel-filtered unlabeled RMA were centrifuged in parallel for 1 h at 90,000 rpm in a TLA100 rotor (Beckman Coulter, Brea, CA). The upper half of each supernatant was carefully removed, actin concentrations were redetermined, and labeled and unlabeled RMA were mixed 1:19. Assembly reactions were 60 µl of final volume and contained final concentrations of 1–3 µM G-actin (5% pyrene labeled). The actin mixture was converted to Mg-ATP-actin ~2 min before use, and then 42 µl of actin was mixed with 15 µl of proteins or control buffer, plus 3 µl of 20× initiation mix (40 mM $MgCl_2$, 10 mM ATP, 1 M KCl) to initiate polymerization. Pyrene fluorescence was monitored at excitation 365 nm and emission 407 nm at 25°C in a fluorescence spectrophotometer (Photon Technology International, Lawrenceville, NJ) or an Infinite M200 plate reader (Tecan, Männedorf, Switzerland). For seeded elongation assays, 10 µM preformed F-actin was freshly sheared and mixed (0.3 µM final) with 0.5 µM monomeric actin (10% pyrene labeled) and 10 nM C-Bni1 ± 200 nM C-Bud6. Two-step seeded nucleation/elongation reactions were performed similarly (explained further in *Results*). Because low concentrations of C-Bni1 and/or C-Bud6 from the first reactions are introduced into the second reactions, we performed control second reactions containing the same final concentrations of C-Bni1 and/or C-Bud6 (without actin seeds from the first reactions). We subtracted the minimal levels of actin assembly observed in these control reactions in order to quantify the increase in actin assembly rate by C-Bni1 and C-Bud6 due to amplification of barbed ends in the first reactions (Figure 2E).

TIRF microscopy

For the TIRF analysis shown in Figure 2, A–C, actin was fluorescently labeled with Alexa 488 (Isambert *et al.*, 1995). Reactions contained 1.2 µM G-actin (30% labeled) ± 5 nM C-Bni1, ± 3.6 µM yeast profilin, ± 0.2 µM C-Bud6. To induce actin polymerization, reaction mixtures were diluted into freshly prepared fluorescence buffer containing 10 mM imidazole-HCl (pH 7.8), 50 mM KCl, 1 mM $MgCl_2$, 100 mM DTT, 3 mg/ml glucose, 20 mg/ml catalase, 100 mg/ml glucose oxidase, and 0.5% methylcellulose. Samples were imaged at 30-s intervals on an Olympus IX-71 inverted microscope equipped with a 60× 1.45 numerical aperture (NA) Plan Apo objective (Olympus; Melville, NY) modified for TIRF illumination as described (Amann and Pollard, 2001). Samples were illuminated with an argon/krypton laser (CVI Melles Griot, Albuquerque, NM) emitting at 488 nm. Images were acquired with a Hamamatsu ORCA-ER camera (Hamamatsu Photonics Deutschland, Herrsching am Ammersee, Germany) running MetaMorph version 6.2r6 software (Universal Imaging, Media, PA).

For the TIRF analysis in Figure 2, E and F, actin was fluorescently labeled with Oregon Green (OG) (Kuhn and Pollard, 2005). Flow cells were first incubated with 20 mM Tris-HCl, pH 8.0, 1% bovine serum albumin (BSA) for 5 min, followed by washing with two chamber volumes 1× TIRF buffer (10 mM imidazole, 50 mM KCl, 1 mM $MgCl_2$, 1 mM EGTA, 0.2 mM ATP, 10 mM DTT, 15 mM glucose, 20 µg/ml catalase, 100 µg/ml glucose oxidase, and 0.5% methylcellulose [4000 cP], pH 7.4). Reactions were initiated by rapidly mixing 1 µM actin (10% OG labeled, 0.5% biotinylated) in 1× TIRF buffer and transferring the reaction to a flow cell. Samples were imaged at 5-s intervals on a Nikon-Ti200 inverted microscope equipped with a 150-mW Ar laser (Mellot Griot, Carlsbad, CA), a TIRF objective with NA of 1.49 (Nikon Instruments, New York, NY), and an iXon EMCCD camera (Andor, Belfast, Northern Ireland). During measurements, optimal focus was maintained using the perfect focus system (Nikon Instruments). The pixel size corresponded to 0.27 µm. The time-lapse movies were analyzed with ImageJ (National Institutes of Health, Bethesda, MD). Elongation rates were determined by measuring the length increase of single filaments over time. Fluorescence intensities of filaments were measured using the ImageJ linescan tool. Bni1-generated filaments were distinguished from spontaneously generated filaments by their ~threefold-faster elongation rates and their 50–70% decrease in fluorescence intensity due to the lower affinity of profilin for OG-labeled actin (Kovar *et al.*, 2006). Bni1-elongated filaments were scored over a time course of 300 s, and each experiment was repeated three times.

Bead pull-down assays

Ni-NTA beads were incubated for 2 h with purified 6His-C-Bni1 and then washed twice with HEKD buffer. Binding reactions contained soluble untagged C-Bud6 and immobilized 6His-C-Bni1 (1 µM each) plus BSA (0.35 mg/ml). In control reactions, empty Ni-NTA beads (no Bni1) were mixed with 1 µM C-Bud6 plus 0.35 mg/ml BSA. Reactions were incubated for 10 min at room temperature, and then beads were pelleted and supernatants were harvested. Beads were washed twice with HEKD. Samples of pellets and supernatants were analyzed on SDS–PAGE gels, and Coomassie-stained bands were quantified using an Odyssey Infrared Imaging System (LI-COR, Lincoln, NE). To determine the relative amount of C-Bud6 depleted from the supernatant, bands corresponding to soluble C-Bud6 in reactions containing Bni1 beads were compared with bands corresponding to soluble C-Bud6 in reactions containing empty beads.

Cell imaging

Yeast strains were grown in YEPD-A (yeast extract, peptone, 2% glucose, 0.15 mM adenine) at 25°C to early log phase and then fixed by incubation with 4% formaldehyde for 45–60 min. Cells were then resuspended in PBS, stained with Alexa 488–phalloidin (Molecular Probes, Eugene, OR), mixed 1:1 with mounting media (9.25 mM *p*-phenylenediamine, 0.02 mg/ml DAPI, 13.7 mM NaCl, 0.27 mM KCl, 0.43 mM Na_2HPO_4, 0.15 mM KH_2PO_4, 90% [vol/vol] glycerol), and imaged on an Axioskop-2 mot *plus* microscope (Carl Zeiss, Thornwood, NJ) equipped with an ORCA-ER digital CCD camera (Hamamatsu Photonics, Bridgewater, NJ). Images were analyzed using OpenLab software (Improvision, Lexington, MA). All images are single planes from fields of view containing at least five cells. Actin phenotypes were scored for large numbers of cells (n > 200) in each strain.

ACKNOWLEDGMENTS

We thank Christopher Gould for technical and intellectual guidance throughout the work and Daqi Tu and Mike Eck for many helpful discussions and insights. This work was supported by National Institutes of Health Grant GM083137 to B.G.

REFERENCES

Amann KJ, Pollard TD (2001). Direct real-time observation of actin filament branching mediated by Arp2/3 complex using total internal reflection fluorescence microscopy. Proc Natl Acad Sci USA 98, 15009–15013.

Amberg DC, Basart E, Botstein D (1995). Defining protein interactions with yeast actin in vivo. Nat Struct Biol 2, 28–35.
Amberg DC, Zahner JE, Mulholland JW, Pringle JR, Botstein D (1997). Aip3p/Bud6p, a yeast actin-interacting protein that is involved in morphogenesis and the selection of bipolar budding sites. Mol Biol Cell 8, 729–753.
Chesarone MA, Goode BL (2009). Actin nucleation and elongation factors: mechanisms and interplay. Curr Opin Cell Biol 21, 28–37.
Dahlgaard K, Raposo AA, Niccoli T, St Johnston D (2007). Capu and Spire assemble a cytoplasmic actin mesh that maintains microtubule organization in the *Drosophila* oocyte. Dev Cell 13, 539–553.
Delgehyr N, Lopes CS, Moir CA, Huisman SM, Segal M (2008). Dissecting the involvement of formins in Bud6p-mediated cortical capture of microtubules in *S. cerevisiae*. J Cell Sci 121, 3803–3814.
Dominguez R (2007). The beta-thymosin/WH2 fold: multifunctionality and structure. Ann NY Acad Sci 1112, 86–94.
Dominguez R (2009). Actin filament nucleation and elongation factors—structure-function relationships. Crit Rev Biochem Mol Biol 44, 351–366.
Evangelista M, Blundell K, Longtine MS, Chow CJ, Adames N, Pringle JR, Peter M, Boone C (1997). Bni1p, a yeast formin linking cdc42p and the actin cytoskeleton during polarized morphogenesis. Science 276, 118–122.
Feierbach B, Verde F, Chang F (2004). Regulation of a formin complex by the microtubule plus end protein tea1p. J Cell Biol 165, 697–707.
Ferron F, Rebowski G, Lee SH, Dominguez R (2007). Structural basis for the recruitment of profilin-actin complexes during filament elongation by Ena/VASP. EMBO J 26, 4597–4606.
Goode BL, Eck MJ (2007). Mechanism and function of formins in the control of actin assembly. Annu Rev Biochem 76, 593–627.
Gould CJ, Maiti S, Michelot A, Graziano BR, Blanchoin L, Goode BL (2011). The formin DAD domain plays dual roles in autoinhibition and actin nucleation. Curr Biol 21, 384–390.
Higashi T, Ikeda T, Murakami T, Shirakawa R, Kawato M, Okawa K, Furuse M, Kimura T, Kita T, Horiuchi H (2010). Flightless-I (Fli-I) regulates the actin assembly activity of diaphanous-related formins (DRFs) Daam1 and mDia1 in cooperation with active Rho GTPase. J Biol Chem 285, 16231–16238.
Higgs HN, Blanchoin L, Pollard TD (1999). Influence of the C terminus of Wiskott-Aldrich syndrome protein (WASp) and the Arp2/3 complex on actin polymerization. Biochemistry 38, 15212–15222.
Isambert H, Venier P, Maggs AC, Fattoum A, Kassab R, Pantaloni D, Carlier MF (1995). Flexibility of actin filaments derived from thermal fluctuationsEffect of bound nucleotide, phalloidin, and muscle regulatory proteins. J Biol Chem 270, 11437–11444.
Jaquenoud M, Peter M (2000). Gic2p may link activated Cdc42p to components involved in actin polarization, including Bni1p and Bud6p (Aip3p). Mol Cell Biol 20, 6244–6258.
Jin H, Amberg DC (2000). The secretory pathway mediates localization of the cell polarity regulator Aip3p/Bud6p. Mol Biol Cell 11, 647–661.
Kikyo M, Tanaka K, Kamei T, Ozaki K, Fujiwara T, Inoue E, Takita Y, Ohya Y, Takai Y (1999). An FH domain-containing Bnr1p is a multifunctional protein interacting with a variety of cytoskeletal proteins in *Saccharomyces cerevisiae*. Oncogene 18, 7046–7054.
Kovar DR, Harris ES, Mahaffy R, Higgs HN, Pollard TD (2006). Control of the assembly of ATP- and ADP-actin by formins and profilin. Cell 124, 423–435.
Kovar DR, Pollard TD (2004). Insertional assembly of actin filament barbed ends in association with formins produces piconewton forces. Proc Natl Acad Sci USA 101, 14725–14730.
Kuhn JR, Pollard TD (2005). Real-time measurements of actin filament polymerization by total internal reflection fluorescence microscopy. Biophys J 88, 1387–1402.
Lee K, Gallop JL, Rambani K, Kirschner MW (2010). Self-assembly of filopodia-like structures on supported lipid bilayers. Science 329, 1341–1345.
Li F, Higgs HN (2003). The mouse Formin mDia1 is a potent actin nucleation factor regulated by autoinhibition. Curr Biol 13, 1335–1340.
Longtine MS, McKenzie A 3rd, Demarini DJ, Shah NG, Wach A, Brachat A, Philippsen P, Pringle JR (1998). Additional modules for versatile and economical PCR-based gene deletion and modification in *Saccharomyces cerevisiae*. Yeast 14, 953–961.
Luedeke C, Frei SB, Sbalzarini I, Schwarz H, Spang A, Barral Y (2005). Septin-dependent compartmentalization of the endoplasmic reticulum during yeast polarized growth. J Cell Biol 169, 897–908.
Moseley JB, Goode BL (2005). Differential activities and regulation of *Saccharomyces cerevisiae* formin proteins Bni1 and Bnr1 by Bud6. J Biol Chem 280, 28023–28033.
Moseley JB, Goode BL (2006). The yeast actin cytoskeleton: from cellular function to biochemical mechanism. Microbiol Mol Biol Rev 70, 605–645.
Moseley JB, Maiti S, Goode BL (2006). Formin proteins: purification and measurement of effects on actin assembly. Methods Enzymol 406, 215–234.
Moseley JB, Sagot I, Manning AL, Xu Y, Eck MJ, Pellman D, Goode BL (2004). A conserved mechanism for Bni1- and mDia1-induced actin assembly and dual regulation of Bni1 by Bud6 and profilin. Mol Biol Cell 15, 896–907.
Nezami A, Poy F, Toms A, Zheng W, Eck MJ (2010). Crystal structure of a complex between amino and carboxy terminal fragments of mDia1: insights into autoinhibition of diaphanous-related formins. PLoS One 5, e12896.
Okada K, Bartolini F, Deaconescu AM, Moseley JB, Dogic Z, Grigorieff N, Gundersen GG, Goode BL (2010). Adenomatous polyposis coli protein nucleates actin assembly and synergizes with the formin mDia1. J Cell Biol 189, 1087–1096.
Otomo T, Tomchick DR, Otomo C, Machius M, Rosen MK (2010). Crystal structure of the formin mDia1 in autoinhibited conformation. PLoS One 5, e12896.
Otomo T, Tomchick DR, Otomo C, Panchal SC, Machius M, Rosen MK (2005). Structural basis of actin filament nucleation and processive capping by a formin homology 2 domain. Nature 433, 488–494.
Padrick SB *et al*. (2008). Hierarchical regulation of WASP/WAVE proteins. Mol Cell 32, 426–438.
Paul AS, Pollard TD (2008). The role of the FH1 domain and profilin in formin-mediated actin-filament elongation and nucleation. Curr Biol 18, 9–19.
Pechlivanis M, Samol A, Kerkhoff E (2009). Identification of a short Spir interaction sequence at the C-terminal end of formin subgroup proteins. J Biol Chem 284, 25324–25333.
Pfender S, Kuznetsov V, Pleiser S, Kerkhoff E, Schuh M (2011). Spire-type actin nucleators cooperate with formin-2 to drive asymmetric oocyte division. Curr Biol 21, 955–960.
Pollard TD, Cooper JA (1984). Quantitative analysis of the effect of *Acanthamoeba* profilin on actin filament nucleation and elongation. Biochemistry 23, 6631–6641.
Prehoda KE, Scott JA, Mullins RD, Lim WA (2000). Integration of multiple signals through cooperative regulation of the N-WASP-Arp2/3 complex. Science 290, 801–806.
Pring M, Evangelista M, Boone C, Yang C, Zigmond SH (2003). Mechanism of formin-induced nucleation of actin filaments. Biochemistry 42, 486–496.
Pruyne D, Evangelista M, Yang C, Bi E, Zigmond S, Bretscher A, Boone C (2002). Role of formins in actin assembly: nucleation and barbed-end association. Science 297, 612–615.
Qualmann B, Kessels MM (2009). New players in actin polymerization—WH2-domain-containing actin nucleators. Trends Cell Biol 19, 276–285.
Quinlan ME, Hilgert S, Bedrossian A, Mullins RD, Kerkhoff E (2007). Regulatory interactions between two actin nucleators, Spire and Cappuccino. J Cell Biol 179, 117–128.
Romero S, Le Clainche C, Didry D, Egile C, Pantaloni D, Carlier MF (2004). Formin is a processive motor that requires profilin to accelerate actin assembly and associated ATP hydrolysis. Cell 119, 419–429.
Rosales-Nieves AE, Johndrow JE, Keller LC, Magie CR, Pinto-Santini DM, Parkhurst SM (2006). Coordination of microtubule and microfilament dynamics by *Drosophila* Rho1, Spire and Cappuccino. Nat Cell Biol 8, 367–376.
Sagot I, Rodal AA, Moseley J, Goode BL, Pellman D (2002). An actin nucleation mechanism mediated by Bni1 and profilin. Nat Cell Biol 4, 626–631.
Segal M, Bloom K, Reed SI (2002). Kar9p-independent microtubule capture at Bud6p cortical sites primes spindle polarity before bud emergence in *Saccharomyces cerevisiae*. Mol Biol Cell 13, 4141–4155.
Shcheprova Z, Baldi S, Frei SB, Gonnet G, Barral Y (2008). A mechanism for asymmetric segregation of age during yeast budding. Nature 454, 728–734.
Sikorski RS, Hieter P (1989). A system of shuttle vectors and yeast host strains designed for efficient manipulation of DNA in *Saccharomyces cerevisiae*. Genetics 122, 19–27.
Spudich JA, Watt S (1971). The regulation of rabbit skeletal muscle contraction. I. Biochemical studies of the interaction of the tropomyosin-troponin complex with actin and the proteolytic fragments of myosin. J Biol Chem 246, 4866–4871.

Theurkauf WE (1994). Premature microtubule-dependent cytoplasmic streaming in cappuccino and spire mutant oocytes. Science 265, 2093–2096.

Tong AH *et al*. (2001). Systematic genetic analysis with ordered arrays of yeast deletion mutants. Science 294, 2364–2368.

Vizcarra CL, Kreutz B, Rodal AA, Toms AV, Lu J, Zheng W, Quinlan ME, Eck MJ (2011). Structure and function of the interacting domains of Spire and Fmn-family formins. Proc Natl Acad Sci USA 108, 11884–11889.

Wen Y, Eng CH, Schmoranzer J, Cabrera-Poch N, Morris EJ, Chen M, Wallar BJ, Alberts AS, Gundersen GG (2004). EB1 and APC bind to mDia to stabilize microtubules downstream of Rho and promote cell migration. Nat Cell Biol 6, 820–830.

Xu Y, Moseley JB, Sagot I, Poy F, Pellman D, Goode BL, Eck MJ (2004). Crystal structures of a Formin Homology-2 domain reveal a tethered dimer architecture. Cell 116, 711–723.

Yang C, Czech L, Gerboth S, Kojima S, Scita G, Svitkina T (2007). Novel roles of formin mDia2 in lamellipodia and filopodia formation in motile cells. PLoS Biol 5, e317.

Zeth K, Pechlivanis M, Samol A, Pleiser S, Vonrhein C, Kerkhoff E (2011). Molecular basis of actin nucleation factor cooperativity: crystal structure of the Spir-1 KIND/formin-2 FSI complex. J Biol Chem.

Zigmond SH, Evangelista M, Boone C, Yang C, Dar AC, Sicheri F, Forkey J, Pring M (2003). Formin leaky cap allows elongation in the presence of tight capping proteins. Curr Biol 13, 1820–1823.